ELSEVIER

Polymer 40 (1999) 3487–3499

polymer

Acetone sorption and uptake kinetic in poly(ethylene terephthalate)

C.C. McDowell[a,*], B.D. Freeman[a], G.W. McNeely[b]

[a]*Department of Chemical Engineering, North Carolina State University, Raleigh, NC 27695-7905, USA*
[b]*Hoechst-Celanese Corporation, Spartanburg, SC, USA*

Received 11 March 1998; received in revised form 8 May 1998; accepted 18 May 1998

Abstract

The sorption and kinetics of acetone uptake in solvent cast films of poly(ethylene terephthalate) are reported at 35°C for acetone pressures ranging from 0 to 7.3 cm Hg. The equilibrium sorption isotherm is well described by the dual-mode sorption model with the following parameters: $k_D = 61$ cm^3(STP)/(cm^3·atm), $C'_H = 7.2$ cm^3(STP)/cm^3, and $b = 50$ atm^{-1}. Sorption kinetics are described using a two-stage model which incorporates both Fickian diffusion and protracted polymer structural relaxation. The characteristic time associated with the relaxation process is essentially independent of acetone concentration and has an average value of approximately 15 hours. The fraction of sorption associated with polymer relaxation increases linearly with acetone concentration in the equilibrium-densified matrix of the polymer. Acetone diffusion coefficients increase with increasing acetone concentration. The concentration dependence of the acetone diffusion coefficient is well described by the dual-mobility model if the assumption of constant diffusion coefficients in the two modes is relaxed.

Keywords: Sorption; Diffusion; Acetone

1. Introduction

Poly(ethylene therephthalate) [PET] is an important barrier material that is widely used to package foods and beverages [1]. An important consideration in barrier packaging applications is the loss of organic flavor molecules, such as d-limonene in fruit juices, as a result of scalping, i.e. sorption of the flavor molecules into package walls [2]. Additionally, flavor molecule carry-over is emerging as a concern for refillable plastic beverage bottles. Flavor molecules sorbed into package walls from an initially-packaged product desorb after refill to influence the taste of the product in the refilled package. To understand better the sorption and transport of flavor components (such as esters, ketones, and aromatics) into barrier polymers such as PET, small organic penetrants are used as model marker molecules [3].

The sorption of organics in PET has been the subject of several investigations. As PET is a glassy polymers, the equilibrium sorption isotherms of a variety of organic vapors, e.g. methanol [4], ethyl acetate [4], and benzene [5], are reported to be well described by the dual-mode sorption model [6] or the so-called generalized dual-mode sorption model [7]. Liu and Neogi measured methylene chloride vapor sorption kinetics in PET over a wide range of penetrant activity and observed Fickian mass uptake kinetics [8]. The sorption isotherm of methylene chloride in PET was well described by the generalized dual-mode model [8]. In another study, the kinetics of benzene uptake in PET were rationalized using a model which combined Fickian diffusion within the context of the dual-mode transport theory (the so-called dual mobility model), and structural relaxation of the polymer upon penetrant sorption, i.e. swelling-controlled penetrant uptake [5]. Sorption of liquid dimethylformamide in PET obeyed Fickian kinetics in a set of films prepared with draw ratios ranging from 1.6 to 4.0 [9].

Durning and Russel proposed a model for diffusion with induced crystallization to describe sorption kinetics of organic liquids which can trigger PET crystallization [10]. In another study, Durning et al. measured sorption and transport of methylene chloride and dimethylformamide in PET films and observed that both polymer swelling and solvent-induced crystallization influence penetrant sorption kinetics [11]. Billovits and Durning found that organic penetrant transport properties in PET were sensitive to film processing conditions [12]. In particular, the sorption kinetics of strongly swelling penetrants such as acetone and

* Corresponding author.

0032-3861/99/$ - see front matter
PII: S0032-3861(98)00403-0

dimethylformamide (DMF) are influenced by thermal annealing and prior exposure to penetrants such as liquid methylene chloride. Initially amorphous PET films were crystallized by exposure to methylene chloride, i.e. solvent-induced crystallization, low temperature annealing (120°C), or high temperature annealing (230°C). The sample annealed at high temperature had the highest level of crystallinity (47 wt%), and the film crystallized by exposure to methylene chloride had the lowest level of crystallinity (23 wt%). DMF diffusion coefficients determined from desorption experiments decreased with increasing crystallinity. For example, at 65°C, the diffusion coefficient of DMF was 74×10^{-9} cm^2 s^{-1} in the film crystallized with methylene chloride and 5×10^{-9} cm^2 s^{-1} in the film annealed at high temperature. DMF sorption kinetics were non-Fickian. At short times, the fractional mass uptake was convex to the $t^{1/2}$ axis. The lengths of the convex portions of the uptake kinetics are reported as induction times, or the time necessary to establish diffusion control of mass uptake. The induction time increased with increasing crystallinity. At longer times, uptake kinetics were a linear function of $t^{1/2}$, where t is the time since the beginning of the experiment, and the slope of the linear region was used to estimate the diffusion coefficient. Like DMF diffusion coefficients, the diffusivity of methylene chloride decreased with increasing crystallinity.

Transport properties of organic molecules such as acetone can be more sensitive than those of smaller molecules, such as carbon dioxide and oxygen, to subtle effects of processing and polymer structure on sorption and transport properties in high barrier polymers [13–15]. Penetrant diffusion coefficients are commonly understood to depend sensitively on free volume in the polymer matrix. One of the most widely used models of the effect of free volume on the penetrant diffusion coefficients, the Cohen–Turnbull model [16], suggests that the diffusion coefficients of larger penetrants are more sensitive than those of smaller penetrants to changes in the amount of free volume in the polymer matrix. The Lennard–Jones diameters of acetone, CO_2, and O_2, are 4.6 Å, 3.94 Å and 3.47 Å, respectively [17]. As acetone is substantially larger than the other two molecules, its diffusion coefficient should be more sensitive than those of O_2 and CO_2 to subtle processing-induced changes in the free volume in the polymer matrix. As a result, several studies have used acetone as a marker organic molecule to probe the effect of polymer chemistry and processing on sorption and transport properties of high barrier polyesters [14,18]. In these studies, the transport properties of acetone were observed to be more strongly influenced by polymer thermal history than the transport properties of small molecules such as O_2 and CO_2 [15].

In this study, the equilibrium uptake and kinetics of acetone sorption in a solution-cast film of PET are reported. The dual-mode model is used to analyze the equilibrium sorption isotherms. An empirical two-stage model incorporating Fickian diffusion and relaxation-controlled kinetics describes the kinetics of acetone uptake. The effect of acetone concentration on acetone diffusion coefficient is analyzed in the context of the dual mobility model [5].

2. Experimental

2.1. Polymer synthesis

PET was synthesized in a two-stage process. Dimethyl terephthalate (5.15 moles), an excess of ethylene glycol, and the catalyst mixture (manganese diacetate, 90 ppm Mn; cobalt diacetate, 90 ppm Co; and antimony trioxide, 350 ppm Sb) were added to a reaction vessel. Heat was applied to begin the ester interchange reaction. The methanol byproduct was removed, and when the reaction temperature had increased to 250°C, the ester interchange was complete.

In the polycondensation stage, a phosphorus-containing stabilizer in the form of polyphosphoric acid (82 ppm P) was added to the ester interchange product, and the pressure was gradually reduced to about 0.1 cm Hg as the temperature was increased to approximately 290°C to obtain the product.

The solution viscosity, percent diethylene glycol [DEG], and percent carboxylic acid were determined for the as-synthesized polymer. The solution viscosity, SV, is given by

$$SV = (\eta_{rel} - 1) \times 100 \quad (1)$$

where η_{rel} is the relative viscosity. The relative viscosity of a 1 wt% solution of the polymer in dichloroacetic acid was measured using a capillary viscometer at 25°C, and Eq. (1) was used to compute solution viscosity. To determine the percentage of diethylene glycol in the final polymer, the polymer sample was first dissolved in 30% NH_4OH by heating in a high pressure vessel at 220°C for 2 hours. This process completely hydrolyzed the sample to monomer. The percent diethylene glycol in the polymer was then determined by gas chromatography using diethylene glycol as a standard. For end group (percent carboxylic acid) analysis, 0.14 g of the sample was dissolved in 6 ml of benzyl alcohol at 206°C. The solution was then titrated with an aqueous KOH solution using phenol red as the indicator.

2.2. Film preparation

A uniform thickness polymer film (5.6 μm thick) was prepared by casting a 5% (w/v) solution of the polymer in trifluoroacetic acid at ambient conditions onto a glass plate, and a doctor blade was used to control film uniformity. The sample was first dried at ambient conditions for 24 hours. Afterwards, the film was soaked in a water bath for 24 hours and then in a methanol bath for 24 hours to remove residual solvent. Following the methanol bath, the film was placed in a vacuum oven for 24 hours at room temperature to

completely remove the solvent. Differential Scanning Calorimetry (DSC) and sensitive gravimetric desorption studies in a vacuum chamber showed no traces of residual solvent in the final film.

2.3. Thermal and physical characterization

A Perkin-Elmer DSC-7 was used at a scan rate of 20°C min^{-1} to characterize thermal transitions of the PET film. The second DSC scan is reported for thermal transition measurements. However, results from the first DSC scan are used for crystallinity measurements to characterize the polymer properties in the as-cast state. A wide-angle X-ray diffraction (WAXD) spectrum was obtained using a Siemens Kristalloflex 4 X-ray Generator and a Siemens type FΘ/2Θ goniometer. The X-rays were produced by a Cu Kα ($\lambda = 1.54$ Å) source. Density measurements were performed with a Techne density gradient column using aqueous calcium nitrate solutions with a density range of approximately 1.2 to 1.5 g cm^{-3}.

2.4. Kinetic gravimetric sorption

The kinetics of acetone sorption were recorded using a Cahn RG-2000 electrobalance at 35°C and a pressure range of 0–7.2 cm Hg. A more detailed description of the experimental procedure is available elsewhere [19]. The film was conditioned by exposure to 7.2 cm Hg of acetone and then degassed prior to the gravimetric sorption studies described in this report. This conditioning protocol alleviates penetrant-induced crystallization during the subsequent sorption experiments. Based on DSC experiments, there was no measurable difference in crystallinity levels in the films before and after sorption.

3. Results and discussion

3.1. Polymer characterization

The solution viscosity of the as-synthesized polymer was 919. From this value, an intrinsic viscosity of 0.70 dL g^{-1} was estimated using a correlation available from Hoechst-Celanese. The concentration of carboxylic acid end groups in the polymer was 40 milliequivalents per kilogram, which corresponds to a number average molecular weight of 25 000 g $mole^{-1}$. The concentration of DEG was 0.86 wt% (based on the total mass of the polymer sample).

A second scan DSC thermogram of an as-cast PET film is presented in Fig. 1. The thermogram exhibits a glass/rubber transition, T_g, at 81°C, a cold crystallization exotherm, T_c, centered at 141°C, and a melting point, T_m, at 255°C. These transition temperatures agree well with literature values for T_g (81°C) and T_m (250–265°C) [20]. As kinetic constraints on macromolecular mobility are relieved at temperatures above T_g, the polymer crystallizes on the time scale of the

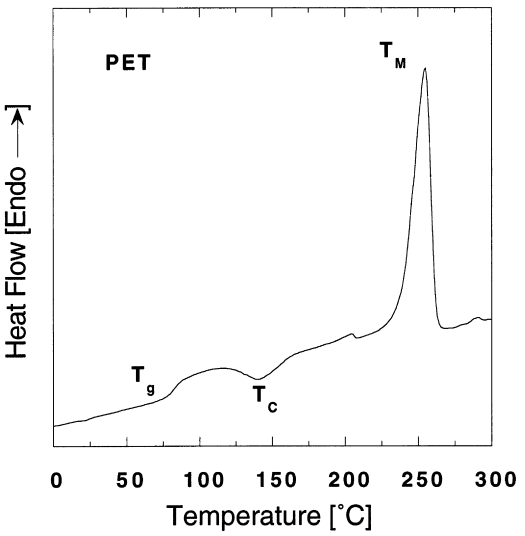

Fig. 1. DSC thermogram of as-cast PET film, scan rate = 20°C min^{-1}.

DSC experiment [21]. Therefore, the cold crystallization exotherm is observed, as expected, above T_g. The weight percent crystallinity was calculated by subtracting the enthalpy of cold crystallization from the enthalpy of melting (both determined by measuring the area under the respective peaks in the DSC thermogram) and dividing by the heat of fusing of PET, 140 J g^{-1} [22]. The weight percent crystallinity is 40%.

Fig. 2 presents a wide-angle X-ray diffraction spectrum of the as-cast PET film. The three strong diffraction peaks centered at $2\theta = 16.4$, 22.0, and 25.1° are associated with PET crystallites. The vertical lines in Fig. 2 represent values of WAXD peak locations expected for the $(0\bar{1}1)$, (010), $(\bar{1}10)$, and (100) reflections in PET [23]. These are the strongest reflections reported in a previous crystallography

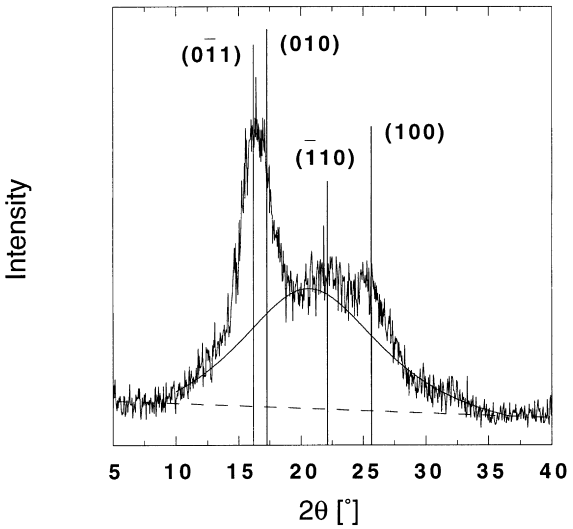

Fig. 2. WAXD spectrum of as-cast PET film. The smooth curve is a Lorentzian function representing the amorphous halo. The dashed line represents the baseline of the spectrum. The vertical lines represent expected diffraction peak locations based on literature reports of the crystal structure of PET [23].

study of PET [23]. The unit cell of PET is triclinic, with one monomer per unit cell, and the following unit cell parameters: $a = 4.56$ Å, $b = 5.94$ Å, $c = 10.75$ Å, $\alpha = 98.5°$, $\beta = 118°$, $\gamma = 112°$ [23]. The broad amorphous halo in the WAXD spectrum is centered at approximately $2\theta = 20.6°$. From this value of 2θ, using Bragg's law [24] ($\lambda = 2d \sin\theta$), the d-spacing of the amorphous material was estimated to be 4.3 Å. Murthy et al. separate the amorphous halo of PET into two peaks, one centered at $2\theta = 17.5°$ (5.0 Å) and the other at 23.5° (3.9 Å) [23]. The peak with a d-spacing of 3.9 Å is ascribed to interchain spacing normal to the plane of aligned aromatic rings in the PET matrix. The peak with a d-spacing of 5.0 Å is attributed to interchain spacing in the plane of the aligned aromatic rings. The relative areas of the two amorphous peaks were used to evaluate the amount of orientation and order in the amorphous PET matrix [23]. The data in Fig. 2 are considered to be consistent with those of Murthy et al. However, in our WAXD spectrum, there is not sufficient resolution to extract definitively two amorphous halos from the spectrum of the semicrystalline sample.

The weight percent crystallinity was estimated to be 38% from the WAXD spectrum in Fig. 2. The value was obtained by computing the areas under the amorphous peak and crystalline peaks after establishing a baseline for the spectrum. The crystalline content was then estimated as $A_C/(A_A + A_C)$ where A_C is the area associated with the crystalline peaks and A_A is the area associated with the amorphous halo.

The density of the film was 1.373 g cm^{-3}. The densities of completely crystalline and wholly amorphous PET are 1.440 and 1.327 g cm^{-3}, respectively [25]. Based on our measured density value, the weight percent crystallinity, X_C, is estimated to be 41% using the relation

$$X_C = (\rho - \rho_A)/(\rho_C - \rho_A) \times 100 \quad (2)$$

where ρ is the polymer density, ρ_A is the density of amorphous PET, and ρ_C is the density of completely crystalline PET. The independent estimates of crystalline from WAXD (38%), DSC (40%), and densitometry (41%) are in excellent agreement.

3.2. Equilibrium acetone uptake

Interval gravimetric sorption experiments were used to determine the sorption isotherm presented in Fig. 3. The shape of this isotherm is typical of that for isotherms of condensable low activity organic vapors in glassy polymers [6], and the isotherm is well-described by the dual mode model [6]

$$C = C_D + C_H \quad (3)$$

where C is the equilibrium concentration of penetrant in the polymer, C_D is the equilibrium concentration of penetrant in the Henry's law mode, and C_H is the equilibrium concentration of penetrant in the Langmuir mode. The analytical

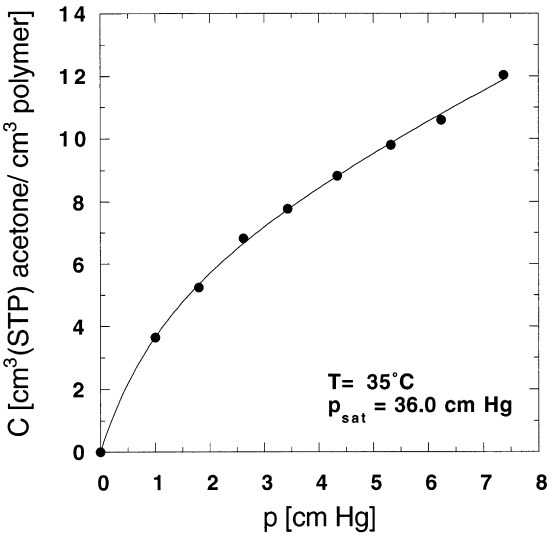

Fig. 3. Acetone sorption isotherm in PET at 35°C.

expressions for C_D and C_H are [6]

$$C_D = k_D p \quad (4)$$

and

$$C_H = \frac{C_H' b p}{1 + bp} \quad (5)$$

so that

$$C = k_D p + \frac{C_H' b p}{1 + bp}. \quad (6)$$

In these expressions, k_D is the Henry's law coefficient, which characterizes equilibrium sorption of the penetrant into the equilibrium densified polymer matrix. The Langmuir capacity parameter, C_H', characterizes penetrant sorption in the non-equilibrium excess volume associated with the glassy polymer matrix. The Langmuir affinity parameter, b, characterizes the affinity of the penetrant for a Langmuir site in the matrix. C_D is, therefore, the equilibrium concentration of penetrant in the densified polymer matrix, and C_H is the equilibrium concentration of penetrant in the non-equilibrium excess volume. The curve in Fig. 3 represents a least-squares fit of the sorption data to the dual-mode model. This non-linear regression yielded the following model parameters: $k_D = 61 \pm 7.4$ cm^3(STP)/(cm^3·atm), $C_H' = 7.2 \pm 1.1$ cm^3(STP)/cm^3 and $b = 50 \pm 12$ atm^{-1}.

The logarithm of gas solubility or Henry's law coefficients of penetrants in both rubbery [26,27] and glassy [28] polymers often increases linearly with penetrant critical temperature. Solubility coefficients for several permanent gases [29], as well as the dual mode parameters for carbon dioxide [30] and benzene [5], in PET are available. The solubility coefficients for the permanent gases and the Henry's law coefficients for CO_2, acetone, and benzene, divided by amorphous volume fraction, Φ_A, to correct for crystallinity [31,32], are presented in Fig. 4a as a function of penetrant critical temperature. The data were collected in

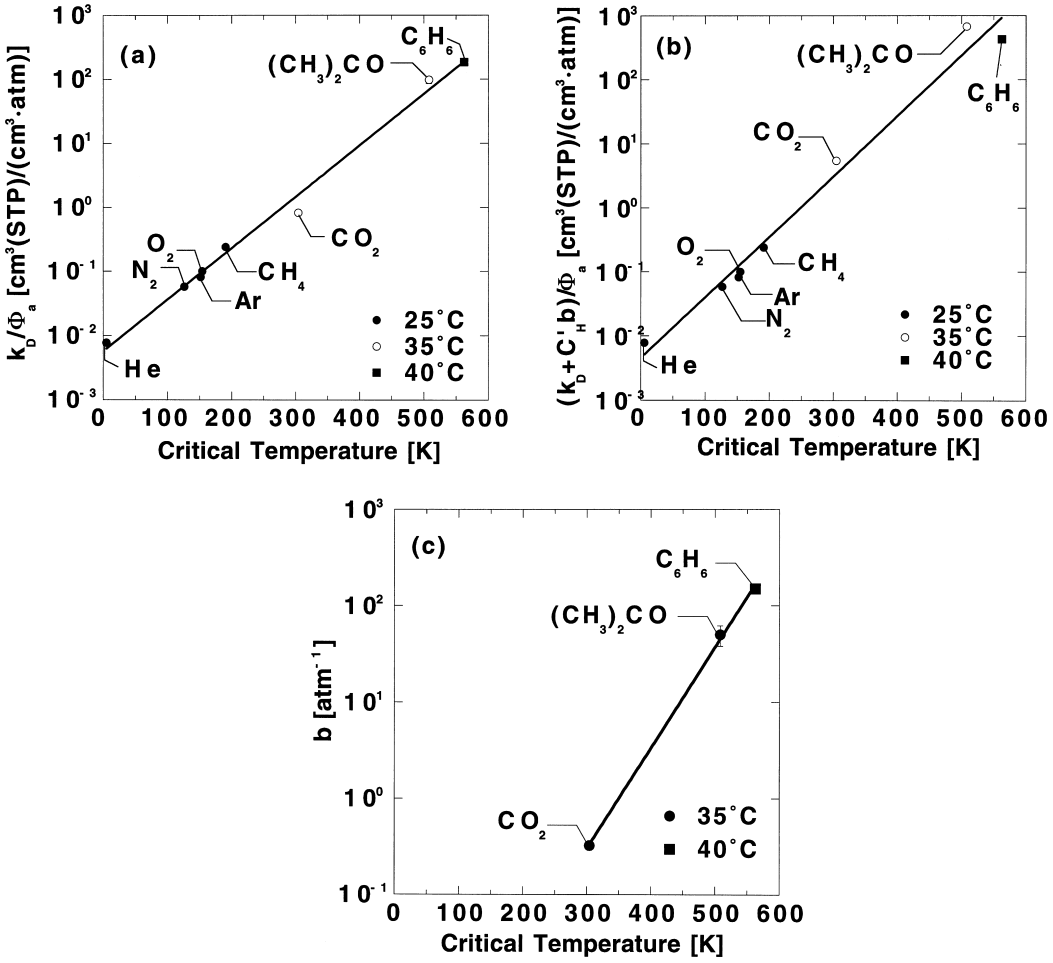

Fig. 4. Dual-mode sorption parameters of PET as a function of penetrant critical temperature: (a) Henry's law parameter, (b) infinite dilution solubility, (c) Langmuir affinity parameter.

different laboratories and at three different temperatures. The correlation is impressive and suggests that the Henry's law coefficient determined in this study is reasonable.

For the permanent gases (He, N_2, Ar, O_2, CH_4), the Henry's law parameter reported in Fig. 4a is actually the infinite dilution solubility, k_D^*, where $k_D^* = k_D + bC_H'$, because sorption isotherms for the permanent gases (He, N_2, Ar, O_2, CH_4) are linear functions of pressure and, consequently, separate estimates for k_D, b, and C_H' are not available. However, for CO_2, acetone, and benzene, bC_H' is at least as large as k_D. Therefore, to provide what is perhaps a more appropriate comparison of the sorption data for different penetrants, Fig. 4b presents the infinite dilution solubility coefficient, k_D^*, versus penetrant critical temperature. The correlation of the data with critical temperature is also excellent, again confirming that the acetone sorption parameters are reasonable.

Langmuir affinity parameters have also been correlated with penetrant critical temperature [33]. In this regard, Fig. 4c presents the Langmuir affinity parameter, b, as a function of critical temperature for carbon dioxide, acetone, and benzene. As with k_D, there is excellent agreement of our acetone Langmuir affinity parameter with those of other penetrants.

3.3. Acetone sorption kinetics

Fig. 5 presents results from four representative acetone kinetic sorption experiments in PET. The time since the penetrant pressure surrounding the polymer sample was increased from its initial value, p_i, to its final value, p_f, is t, M_t is the mass of acetone sorbed by the polymer from the beginning of the experiment until t, and M_∞ is the equilibrium mass uptake during the interval sorption experiment. At short times, the fractional mass uptake, M_t/M_∞, increases linearly with $t^{1/2}$, which is characteristic of sorption kinetics controlled by Fickian diffusion [34]. At longer times, the mass uptake exhibits a protracted, non-Fickian asymptotic approach towards equilibrium. Such so-called two stage kinetics [35] are often observed for organic vapor sorption in glassy polymers. Examples include vinyl chloride monomer in PVC [36], benzene in PET [5], methyl acetate in polymethyl methacrylate and cellulose acetate [37], benzene in polystyrene [37], acetone in cellulose nitrate

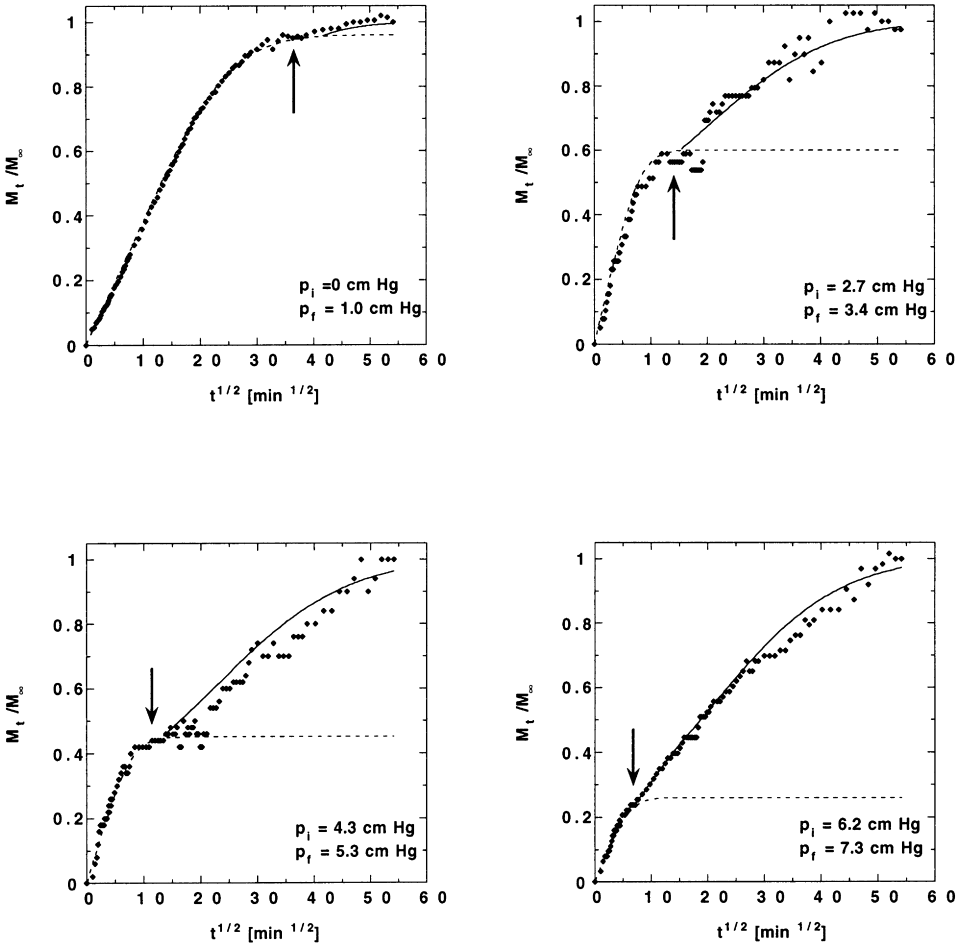

Fig. 5. Examples of interval acetone sorption kinetics in PET at 35°C. The dashed line is the contribution of Fickian-controlled mass uptake kinetics, and the solid line represents the contribution of relaxation-controlled uptake kinetics to the overall mass uptake.

[37], and ethyl benzene in polystyrene [38]. Often, such sorption kinetics are described using the following empirical model [36]

$$\frac{M_t}{M_\infty} = 1 - (1-\alpha_R)\frac{8}{\pi^2}\sum_{n=0}^{\infty}\frac{1}{(2n+1)^2} \exp\left(\frac{-\bar{D}(2n+1)^2\pi^2 t}{\ell^2}\right) - \alpha_R \exp\left(\frac{-t}{\tau_R}\right) \quad (7)$$

where $\bar{D}$ is the average diffusion coefficient (defined below), α_R is the fraction of weight uptake occurring during the protracted, non-Fickian approach to equilibrium, and τ_R is the time constant associated with the long time drift in mass uptake [5]. The long-term drift in sorption kinetics is usually ascribed to mass uptake controlled by the viscoelastic relaxation of the polymer chains to accommodate penetrant [5]. $\bar{D}$ is approximately equal to the average effective diffusion coefficient over the concentration interval of the experiment [35]:

$$\bar{D} = \frac{1}{C_f - C_i}\int_{C_i}^{C_f} D(C)\mathrm{d}C \quad (8)$$

where C_i and C_f are penetrant concentrations in the polymer at the beginning and end of the sorption experiment, and $D(C)$ is the effective diffusion coefficient.

Fig. 6 presents a least squares fit of Eq. (7) to the experimental data for an acetone pressure interval from 1.8 cm Hg to 2.7 cm Hg. While Eq. (7) can describe the data, from this best fit, α_R is 0.60, suggesting that 60% of the mass uptake is controlled by relaxation. In contrast, M_t/M_∞ is linear with $t^{1/2}$ at short times and approaches a plateau at $M_t/M_\infty \approx 0.72$. Afterwards, there is a second stage of uptake which is not a linear function of $t^{1/2}$. Based on this qualitative examination of the experimental data, and in contrast to the result of the least square fit of Eq. (7) to the data, Fickian diffusion controls the initial 72% of mass uptake, and the remaining 28% is controlled by polymer relaxation. Additionally, the value of $\bar{D}$ from the best fit of Eq. (6) to the data is 8.2×10^{-12} cm^2 s^{-1}, which is approximately three times higher than would be expected from the initial slope of the data in Fig. 6. That is, a fit of Eq. (7) to the data in Fig. 6 fails to provide reasonable parameter values.

For the simple empirical model represented in Eq. (7), diffusion and relaxation occur in parallel, and therefore, the

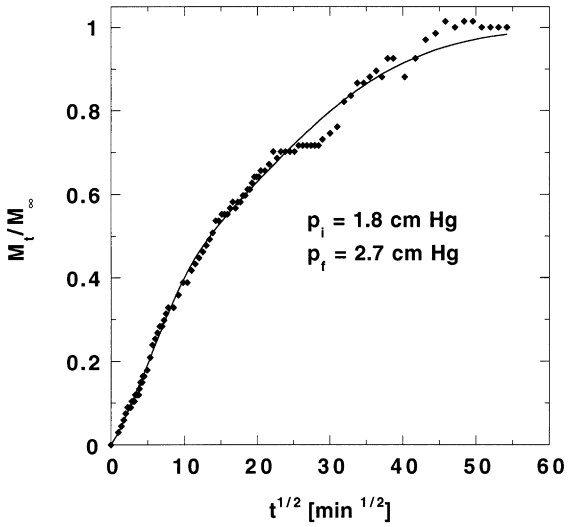

Fig. 6. Fit of Eq. (7) to interval kinetic sorption data for acetone in PET.

faster process controls initial mass uptake. Based on the linearity of initial uptake with $t^{1/2}$ in Figs. 5 and 6, diffusion controls initial mass uptake for each pressure interval. The model, however, only describes two-stage kinetics (with diffusion controlling the first stage) if the long-time relaxation process is much slower than the diffusion process controlling initial uptake kinetics. As demonstrated below, the timescale for diffusion is actually longer than the timescale for relaxation for the data in Fig. 6. Eq. (7) cannot describe two-stage mass uptake kinetics when the second stage, i.e. relaxation, occurs in series with a diffusion-controlled first stage and the relaxation timescale is faster than the diffusion timescale. The first three pressure intervals explored in this study (0–1.0, 1.0–1.8, and 1.8–2.7 cm Hg) are in this category. Therefore, the method described below was used to characterize the sorption kinetics for each interval.

At each pressure interval, the diffusion-controlled process is essentially complete before polymer relaxation rate-controlled mass uptake begins. The presence of an intermediate plateau region in each graph in Fig. 5 (indicated by arrows) between the diffusion-controlled and relaxation-controlled regimes of mass transfer is consistent with this simplified view of the kinetics of acetone sorption in PET and permits a separation of the two processes.

The fraction of weight uptake controlled by Fickian diffusion, $(1 - \alpha_R)$, is estimated as the fraction of weight uptake at the intermediate plateau of the sorption data. The Fickian diffusion coefficient is estimated from a least squares fit of the data (from $t = 0$ to the Fickian plateau) to the model for diffusion in a uniform plane sheet [35]

$$\frac{\frac{M_t}{M_\infty}}{(1-\alpha_R)} = 1 - \frac{8}{\pi^2}\sum_{n=0}^{\infty}\frac{1}{(2n+1)^2}\exp\left(\frac{-\bar{D}(2n+1)^2\pi^2 t}{\ell^2}\right). \tag{9}$$

Fig. 7 presents a characteristic example of a non-linear least square fit of the data to Eq. (9) for the acetone partial pressure interval from 1.8 to 2.7 cm Hg.

For this same kinetic sorption experiment, Fig. 8 illustrates the procedure for estimating a first-order time constant, τ_R, which characterizes the non-Fickian drift in mass uptake towards equilibrium after the initial diffusion-controlled regime. In the spirit of the model embodied in Eq. (7), polymer relaxation-controlled mass uptake is described as a single exponential

$$\ln\left(1 - \frac{M_t}{M_\infty}\right) = \ln\alpha_R - \frac{t}{\tau_R}. \tag{10}$$

The curves in Fig. 5 represent the separate diffusion and relaxation contributions to the acetone sorption kinetics as determined from Eq. (9) and (10). The values of α_R determined from Eq. (10) are higher than the values determined from the plateaus in Fig. 5. For example, α_R determined

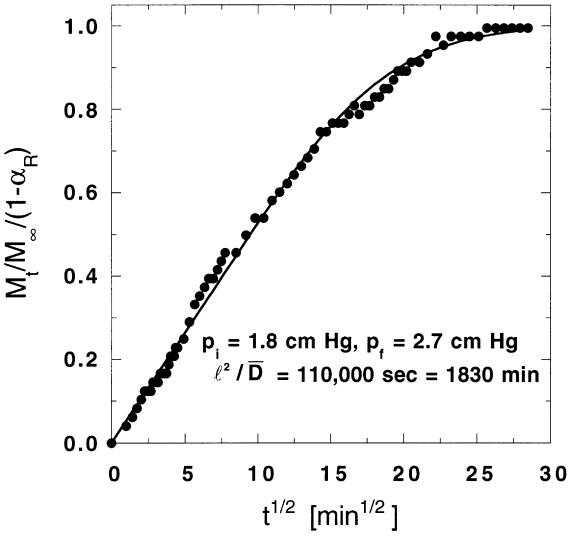

Fig. 7. Analysis of Fickian contribution to acetone sorption kinetics in PET.

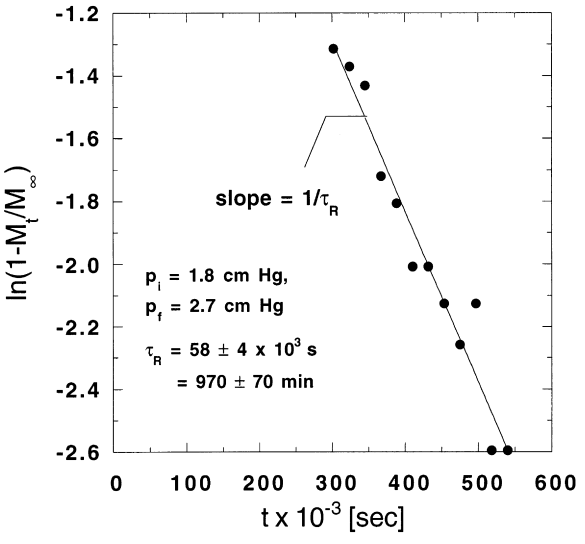

Fig. 8. Analysis of relaxation contribution to acetone sorption kinetics in PET.

from the data in Fig. 8 is 1.4 ± 0.3, which is not consistent with the model, since α_R must lie between zero and one. Moreover, the plateau in the mass uptake data occurs at 0.72, i.e. $1 - \alpha_R = 0.72$, which suggests an α_R value of 0.28. The graphically estimated plateau value is consistently lower than the value determined from Eq. (10) for every pressure interval except the two highest intervals.

If the relaxation process did not begin at $t = 0$ but, rather, started at some later time, then the data would be poorly described by Eq. (7), which assumes that relaxation and diffusion occur simultaneously. Also, as described below, the values for α_R estimated from Eq. (10) would be too high. The notion of a delay in the start of the relaxation process can be included simply in this empirical model by adding a delay time, t_D, to the second term of Eq. (10), which would then be written as follows

$$\ln(1 - \frac{M_t}{M_\infty}) = \left[\ln\alpha_R + \frac{t_D}{\tau_R}\right] - \frac{t}{\tau_R} \quad (11)$$

Initially, the mass uptake is controlled by Fickian diffusion, and the time for half of the total mass uptake controlled by Fickian diffusion to occur is given by [39]

$$t_{1/2} = \frac{\ell^2}{20\bar{D}} = \frac{\tau_D}{20} \quad (12)$$

where τ_D, the characteristic timescale for diffusion, is defined as $\ell^2/\bar{D}$. In all cases except for the two highest pressure intervals, the delay time estimated by Eq. (11) is at least twice the halftime for diffusion, $t_{1/2}$. Therefore, more than 80% of the mass uptake controlled by diffusion appears to be complete before the relaxation-controlled mass uptake begins. Within the context of this simple empirical model (Eq. (11)), this result is consistent with the notion that, for most of the pressure intervals considered, the diffusion-controlled process is essentially complete before relaxation-controlled mass uptake begins. For the two highest pressure intervals, the matrix may contain sufficient acetone and have, therefore, sufficiently high chain mobility, to permit the relaxation process to begin at or near $t = 0$.

The plateau value of mass uptake indicated by the arrows in Fig. 5 is used to estimate α_R for each pressure interval. Eqs. (9) and (11) are used to estimate $\bar{D}$ and τ_R, respectively.

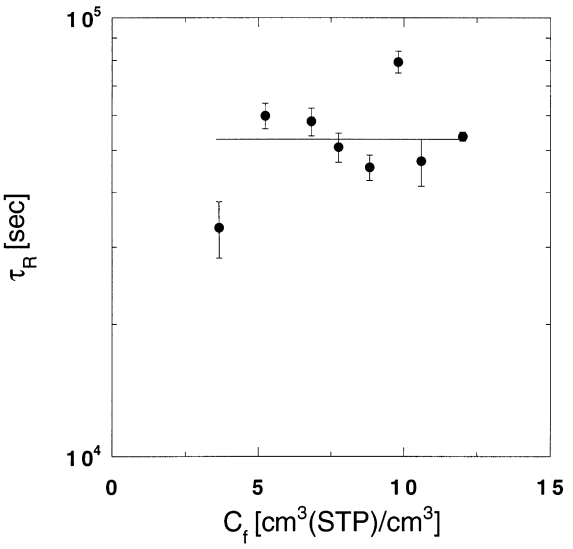

Fig. 9. Characteristic time of relaxation during incremental acetone sorption as a function of final acetone concentration.

The parameter values are recorded in Table 1 along with the Deborah number for diffusion, which is defined as τ_R/τ_D [12]. This dimensionless parameter characterizes the time scale for mass uptake due to structural relaxation relative to the timescale for Fickian diffusion [12]. The uncertainty in the diffusion coefficients in Table 1 is largely due to the uncertainty in determining sample thickness. Uncertainties in the parameters are estimated by the propagation of errors method described by Bevington [40].

Fig. 9 presents the structural relaxation time constant, τ_R, as a function of acetone concentration in the polymer at the end of each kinetic gravimetric sorption experiment, C_f. The relaxation time does not vary systematically over the range of acetone concentration investigated and has an average value of 53 000 ± 4000 seconds. From Table 1, the diffusion Deborah number is less than one for the first three intervals (0–1.0, 1.0–1.8, and 1.8–2.7 cm Hg) and greater than one for the other pressure intervals. The increase in Deborah number results from the increase in acetone diffusion coefficient as acetone concentration increases.

Table 1
Parameters from analysis of the kinetics of acetone sorption in PET

Pressure [cm Hg] p_i	p_f	$\bar{D} \times 10^{12}$ [$cm^2\ s^{-1}$]	α_R	$\tau_R \times 10^{-3}$ [s]	$\tau_D \times 10^{-3}$ [s]	Deborah number (τ_R/τ_D)
0	1.0	1.6 ± 0.1	0.04	33 ± 5	190	0.17
1.0	1.8	2.1 ± 0.2	0.10	60 ± 4	150	0.40
1.8	2.7	2.8 ± 0.3	0.28	58 ± 4	110	0.52
2.7	3.4	13 ± 1.2	0.40	51 ± 4	24	2.1
3.4	4.3	7.6 ± 0.7	0.45	46 ± 3	41	1.1
4.3	5.3	17 ± 1.6	0.55	79 ± 5	18	4.4
5.3	6.2	24 ± 2.1	0.76	47 ± 6	13	3.6
6.2	7.3	28 ± 2.4	0.74	54 ± 1	11	4.8

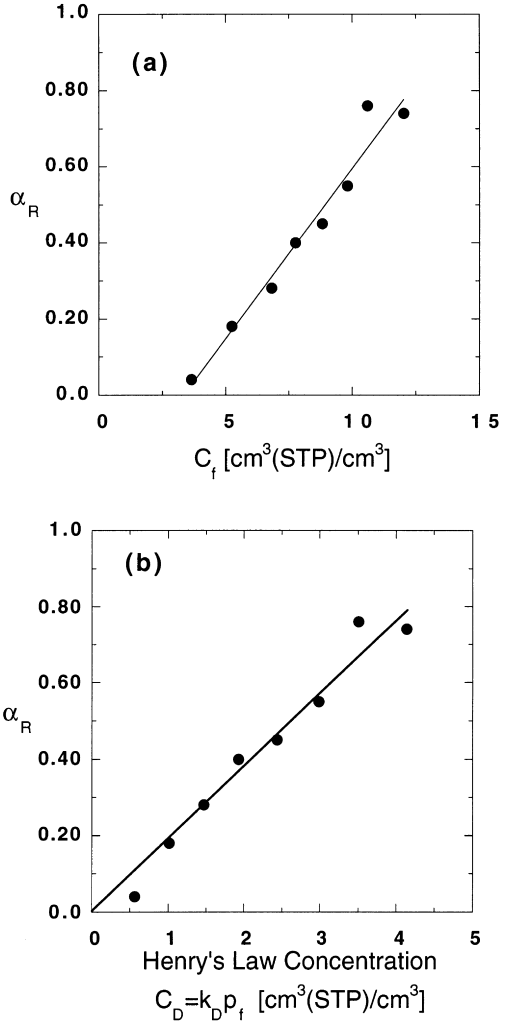

Fig. 10. Effect of acetone concentration on fraction of acetone sorption in PET associated with polymer relaxation: (a) effect of total acetone concentration, (b) effect of Henry's law acetone concentration.

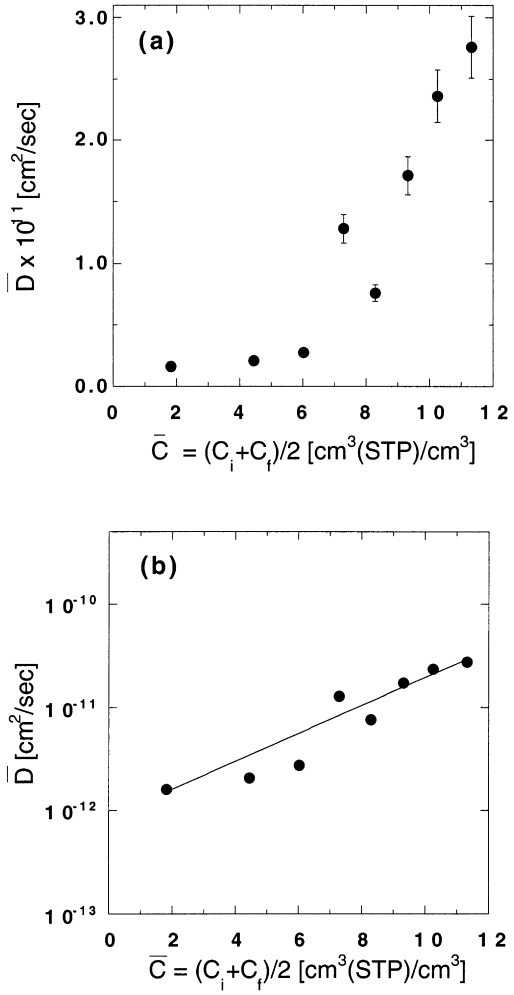

Fig. 11. Acetone diffusion coefficient in PET as a function of average acetone concentration: (a) linear scale, (b) semi-logarithmic scale.

Fig. 10a presents the fraction of mass uptake controlled by relaxation as a function of acetone concentration in the polymer film at the end of each experiment. The value of α_R increases linearly with concentration and has a non-zero intercept. Interestingly, if α_R is presented as a function of acetone concentration in the Henry's law mode (see Fig. 10b), the best line describing the data passes through the origin, suggesting a strong correlation between the concentration of acetone in the Henry's law mode and the fraction of sorption controlled by structural relaxation. It is interesting that in conventional glassy polymers, such as polycarbonate, only penetrant molecules dissolved in the Henry's law mode are understood to contribute to penetrant-induced swelling of the polymer matrix [41].

Fig. 11a presents the dependence of the acetone diffusion coefficient on average acetone concentration during each interval sorption experiment. For lower values of average acetone concentration, i.e. 1.5–6.0 cm^3(STP) acetone/cm^3 polymer, acetone diffusion coefficients increase weakly with increasing acetone concentration. However, at higher acetone concentrations, the acetone diffusion coefficient increases more strongly with increasing concentration. C_i is the acetone concentration at the beginning of an interval sorption experiment, C_f is the acetone concentration at the end of an interval sorption experiment, and $\bar{C}$ is the average of C_i and C_f.

Fig. 11b presents the diffusivity values on a semi-logarithmic scale. An exponential dependence of diffusivity on penetrant concentration is consistent with other reports of the concentration dependence of diffusion coefficients of organic vapors in glassy [42] and rubbery [43] polymers. The diffusivity is often expressed as the following empirical function of average concentration, $\bar{C}$ [44]

$$\bar{D} = D_o e^{\beta \bar{C}} \tag{13}$$

where D_o is the infinite dilution diffusion coefficient and β is an exponential factor describing the dependence of diffusion coefficient on concentration. The values of D_o and β are $9 \pm 5 \times 10^{-12}$ cm^2 s^{-1} and 0.31 ± 0.05 cm^3 cm^{-3}(STP), respectively, based on a least squares fit of the data in Fig. 11b to Eq. (13).

3.4. Dual mobility analysis

A more fundamental model of the concentration dependence of diffusivity in glassy polymers is based on the notion that the two populations of penetrant molecules (Henry's law and Langmuir) in the dual-mode theory have different mobilities [45]. In this so-called dual mobility model, one-dimensional penetrant transport is described by the following form of Fick's law [45]

$$N = -D_H \frac{dC_H}{dx} - D_D \frac{dC_D}{dx} \tag{14}$$

where N is penetrant flux, C_D and D_D are the penetrant concentration and diffusion coefficient in the dense, equilibrium polymer matrix (Henry's law mode), and C_H and D_H are the penetrant concentration and diffusion coefficient in the non-equilibrium excess volume (Langmuir mode).

Within the context of the dual mobility model, the average effective diffusion coefficient determined in kinetic gravimetric sorption experiments is given by [5]

$$\bar{D} = D_D \left[\frac{1 + FK/(1+bp_i)(1+bp_f)}{1 + K/(1+bp_i)(1+bp_f)} \right] \tag{15}$$

where $K = C_H' b/k_D$, and $F = D_H/D_D$. D_H and D_D are assumed to be independent of concentration. If this model adequately describes the experimental data, a plot of $\bar{D}[1 + K/(1+bp_i)(1+bp_f)]$ versus $K/[(1 + bp_i)(1 + bp_f)]$ yields a straight line of slope D_H and intercept D_D. Such behavior has been reported for the diffusion of benzene in PET [5].

Fig. 12 presents our acetone diffusion coefficients plotted in the manner just described. A straight line describes the three data points at lowest acetone concentration, yielding $D_H = 6.4 \pm 5.3 \times 10^{-13}\,cm^2\,s^{-1}$ and $D_D = 96 \pm 2 \times 10^{-13}\,cm^2\,s^{-1}$. However, at higher acetone concentration, this model does not adequately represent the experimental data, suggesting that acetone plasticizes the polymer matrix, thereby increasing D_D and/or D_H.

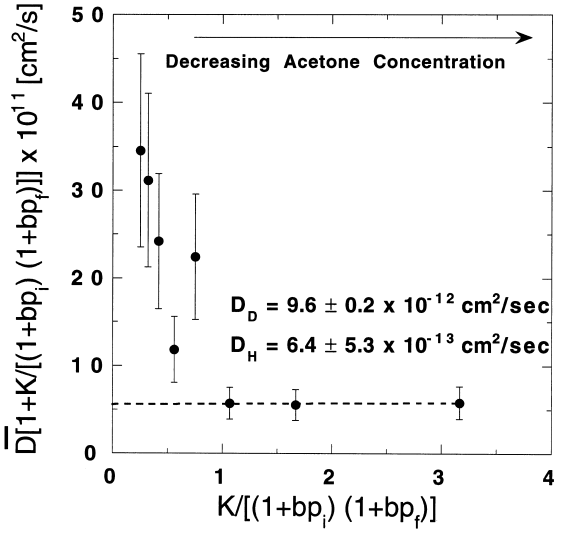

Fig. 12. Dual mobility analysis of acetone diffusion in PET.

Stern and Saxena [46] presented a model to relax the assumption of constant, i.e. concentration independent, D_D and D_H. In the model proposed by Stern and Saxena, both D_D and D_H are presumed to be a function of the effective concentration C_m, where $C_m = C_D + FC_H$, and F is the ratio of D_H and D_D, which is taken to be a constant. A more general model where D_D and D_H have independent concentration dependencies is presented below. The Stern and Saxena model is equivalent to the model described below when the ratio of D_H and D_D is held constant, and the diffusion coefficients are presumed to depend exponentially on the effective concentration, C_m.

Using Eq. (14), the steady state permeability of a penetrant in a glassy polymer may be written as follows [44]

$$P = \frac{\ell}{p_f - p_i} \left[-D_D \frac{dC_D}{dx} - D_H \frac{dC_H}{dx} \right] \tag{16}$$

where ℓ is the film thickness, p_f is the upstream pressure (at $x = 0$) and p_i is the downstream pressure (at $x = \ell$). This expression can be integrated from $x = 0$ to ℓ to give

$$P = \frac{1}{p_f - p_i} \left[\int_{C_{D_i}}^{C_{D_f}} D_D dC_D + \int_{C_{H_i}}^{C_{H_f}} D_H dC_H \right] \tag{17}$$

where C_{D_f} and C_{H_f} are the concentrations of penetrant dissolved in the Henry's law and Langmuir modes at pressure p_f, and C_{D_i} and C_{H_i} are the concentrations of penetrant dissolved in the Henry's law and Langmuir modes at pressure p_i. The permeability can also be defined in terms of the average diffusion coefficient [44]

$$P = \frac{1}{p_f - p_i} \bar{D}(C_f - C_i). \tag{18}$$

Combining Eq. (17) and (18) yields the following relationship

$$\bar{D} = \frac{1}{C_f - C_i} \left[\int_{C_{D_i}}^{C_{D_f}} D_D dC_D + \int_{C_{H_i}}^{C_{H_f}} D_H dC_H \right]. \tag{19}$$

If $\bar{D}_D$ and $\bar{D}_H$ are defined by

$$\bar{D}_D = \frac{1}{C_{D_f} - C_{D_i}} \int_{C_{D_i}}^{C_{D_f}} D_D dC_D \tag{20}$$

and

$$\bar{D}_H = \frac{1}{C_{H_f} - C_{H_i}} \int_{C_{H_i}}^{C_{H_f}} D_H dC_H \tag{21}$$

then Eq. (20) and (21) may be substituted into Eq. (19)

to give

$$\bar{D} = \frac{1}{C_f - C_i}[(C_{D_f} - C_{D_i})\bar{D}_D + (C_{H_f} - C_{H_i})\bar{D}_H] \quad (22)$$

Writing the penetrant concentrations in terms of pressure yields

$$\bar{D} = \frac{1}{(k_D p_f - k_D p_i) - (\frac{C_H' b p_f}{1+bp_f} - \frac{C_h' b p_i}{1+bp_i})} \times \left[(k_D p_f - k_D p_i)\bar{D}_D + (\frac{C_H' b p_f}{1+bp_f} - \frac{C_H' b p_i}{1+bp_i})\bar{D}_H\right]. \quad (23)$$

Eq. (23) reduces to Eq. (15) when $\bar{D}_H$ and $\bar{D}_D$ are constants. $\bar{D}$ is measured experimentally and the other model diffusion coefficients ($\bar{D}_H$ and $\bar{D}_D$) in Eq. (23) are fitted parameters. If $\bar{D}_H$ is arbitrarily assumed to be constant at the value determined from the dual mobility analysis, $6.4 \times 10^{-13}\,cm^2\,s^{-1}$, the effect of acetone concentration on $\bar{D}_D$ can be determined using the equation

$$\bar{D}_D = \frac{\bar{D}[(k_D p_f - k_D p_i) - (\frac{C_H' b p_f}{1+bp_f} - \frac{C_H' b p_i}{1+bp_i})] - (\frac{C_H' b p_f}{1+bp_f} - \frac{C_H' b p_i}{1+bp_i})\bar{D}_H}{(k_D p_f - k_D p_i)}. \quad (24)$$

The results of this analysis are presented in Fig. 13a. The average Henry's law diffusion coefficients are reported as a function of average concentration in the Henry's law regions, $\bar{C}_D$, which is defined as $\bar{C}_D = \frac{1}{2}(k_D p_f + k_D p_i)$. The data are fit to an exponential relationship of the form

$$\bar{D}_D = D_{D_o} e^{\beta_D \bar{C}_D} \quad (25)$$

where D_{D_o} is $7.9 \pm 2.6 \times 10^{-12}\,cm^2\,s^{-1}$ and β_D is $0.32 \pm 0.08\,cm^3\,cm^{-3}$(STP). The value of D_{D_o} agrees well with the value of $\bar{D}_D$ determined by the classical dual mobility analysis at low concentration, $9.6 \pm 0.2 \times 10^{-12}\,cm^2\,s^{-1}$. These values also agree well with the values determined from Fig. 11b, where acetone diffusivity was related to overall average acetone concentration.

At the other extreme, one could assume that $\bar{D}_D$ is constant and confine all concentration dependence of the diffusivity to $\bar{D}_H$. In the following calculations, $\bar{D}_D$ is set to $9.6 \times 10^{-12}\,cm^2\,s^{-1}$, the value obtained from the dual mobility analysis of the low concentration data. The value of $\bar{D}_H$ can be calculated using the equation

$$\bar{D}_H = \frac{\bar{D}(k_D(p_f - p_i) + C_H'(\frac{bp_f}{1+bp_f} - \frac{bp_i}{1+bp_i})) - k_D(p_f - p_i)\bar{D}_D}{C_H'(\frac{bp_f}{1+bp_f} - \frac{bp_i}{1+bp_i})}. \quad (26)$$

These data are presented in Fig. 13b as a function of $\bar{C}_H$, the average concentration of penetrant in the Henry's law mode. These data may be fit to

$$\bar{D}_H = D_{H_o} e^{\beta_H \bar{C}_H} \quad (27)$$

where $D_{H_o} = 1.0 \pm 0.9 \times 10^{-15}\,cm^2\,s^{-1}$ and $\beta_H = 2.0 \pm 0.2\,cm^3\,cm^{-3}$(STP). The value of D_{H_o} is very low and does not agree well with the value of D_H ($6.4 \times 10^{-13}\,cm^2\,s^{-1}$) from the dual mobility analysis of the low concentration data. In addition, the value of β_H is almost an order of magnitude larger than the value of β determined from Fig. 11b, where acetone diffusivity is related to overall average acetone concentration. Based on the magnitudes of the model parameters obtained using these two approaches, the relationship between concentration and diffusivity in Eq. (25) yields more realistic values than the model in Eq. (27).

Using the experimentally determined parameters for D_{D_o} and β_D and substituting Eq. (25) into Eq. (23), the effect of concentration on acetone diffusion coefficient can be described within the context of the modified dual mobility model. A comparison of the model and the experimental data is presented in Fig. 14. The error bars for the three data points at lowest average concentration are smaller than the size of the data points. In general, the data and the model agree well.

Two models have been compared to describe the concentration dependence of acetone diffusivity on acetone concentration in PET, an exponential dependence of diffusivity on concentration (Eq. (13)) and the modified dual mobility model (Eq. (24)). For the empirical model given by Eq. (13), only two adjustable parameters are required to describe the data. The dual mobility model also provides a reasonable

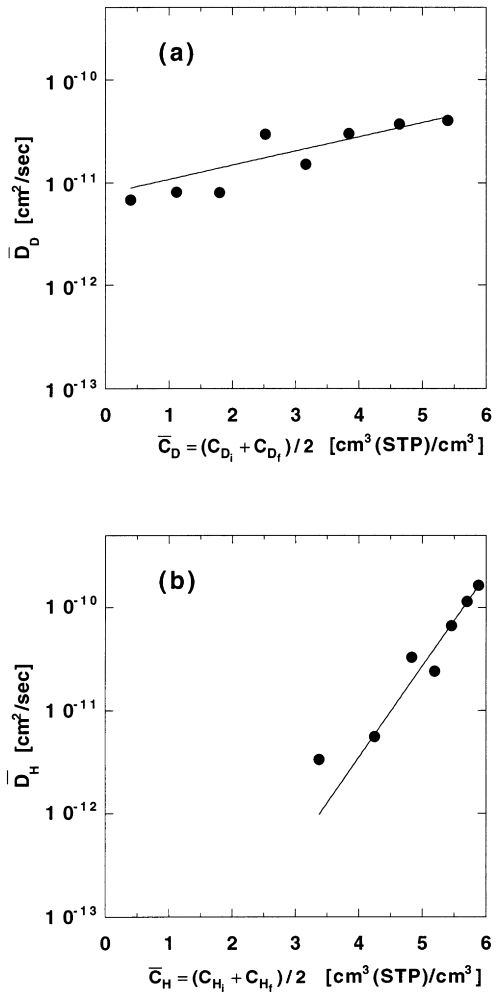

Fig. 13. Dependence of diffusivity on acetone concentration: (a) acetone diffusivity in Henry's law regions as a function of average acetone concentration in Henry's law regions, (b) acetone diffusivity in Langmuir regions as a function of average acetone concentration in Langmuir regions.

description of the experimental data if the assumption of constant Henry's law diffusion coefficient is relaxed. However, the dual mobility model does not provide guidance for the selection of the functional form of the concentration dependence of $\bar{D}_D$. In this study, we have elected to use the empirical expression given by Eq. (24). However, it might prove useful and more satisfying from a theoretical point of view to combine the approach used in free volume theory to predict the concentration dependence of diffusivity [47] with the dual mobility model to obtain a more fundamental model for the concentration dependence of diffusion coefficients of organic vapors in glassy polymers. It would also be of interest to perform the experiments with samples of varying thickness to further decouple the contributions of polymer structural relaxation and Fickian diffusion to overall penetrant uptake in such glassy polymers. However, such studies should also be complemented by a systematic exploration of the effect of thermal history on properties of samples of different thicknesses since preparation of films of different thickness invariably results

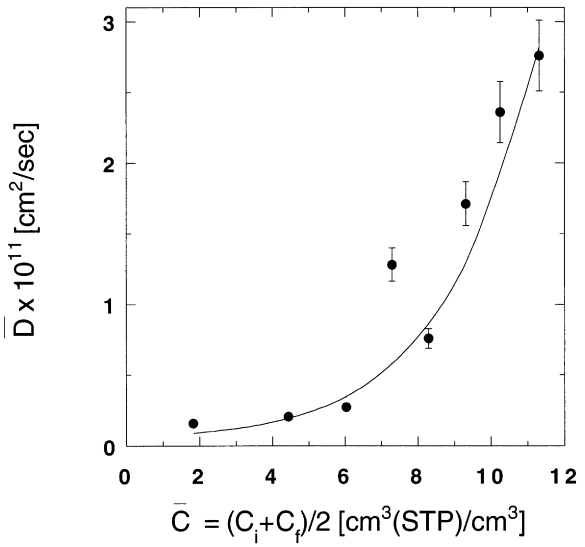

Fig. 14. Composition dependence of acetone diffusivity and fit of the modified dual mobility model.

in variations in processing history which influence chain packing in the solid state of glassy polymers such as PET, and penetrant sorption properties are influenced by such variations in chain packing.

4. Conclusions

The dual-mode model adequately describes the equilibrium sorption of acetone in PET. Interval kinetic gravimetric sorption results are described by an empirical two-stage model, with Fickian diffusion and polymer structural relaxation contributing to the control of mass uptake kinetics. The time constant of the relaxation process does not vary systematically with acetone concentration and has an average value of 53 000 ± 4000 seconds (approximately 15 hours). The fraction of mass uptake associated with the relaxation process increases linearly with increasing concentration of acetone dissolved in the equilibrium-densified region of the polymer matrix.

Acetone diffusivity increases with increasing concentration of acetone dissolved in the PET film. The standard dual mobility model cannot adequately account for this increase, implying that the acetone-induced polymer plasticization plays an important role in the acetone diffusion. However, the experimental data were well described by an extended version of the dual mobility model where the diffusion coefficient of acetone in the Henry's law mode depends exponentially on concentration.

Acknowledgements

The authors gratefully acknowledge the Hoechst Celanese Corporation and the National Science Foundation (Young Investigator Award CTS-9257911-BDF)) for partial

support of this study. In addition, the assistance of Ranjit Mathur and Jason Partin in the laboratory and helpful discussions with Professor C.M. Balik regarding WAXD interpretation were greatly appreciated.

References

[1] Myers J. Modern plastics 1994;40.
[2] Koros WJ. In: Koros WJ, editor. Barrier polymers and structures. Washington, DC: American Chemical Society, 1990:60.
[3] Strandburg G, DeLassus PT, Howell BA. In: Koros WJ, editor. Barrier polymers and structures. Washington, DC: American Chemical Society, 1990:333.
[4] Izydorczyk J, Salwiniski J. Polish Journal of Chemistry 1993;66:321.
[5] Patton CJ, Felder RM, Koros WJ. J Appl Poly Sci 1984;29:1095.
[6] Paul DR. Ber. Bunsenges. Phys. Chem. 1979;83:294.
[7] Berens AR. In: Koros WJ, editor. Barrier polymers and structures. Washington, DC: American Chemical Society, 1990:92.
[8] Liu C-PA, Neogi P. J Macromol Sci Phys 1992;31:265.
[9] Jameel H, Waldman J, Rebenfeld L. J Appl Poly Sci 1981;26:1795.
[10] Durning CJ, Russel WB. Polymer 1985;26:131.
[11] Durning CJ, Rebenfeld L, Russel WB. Pol Eng Sci 1986;26:1066.
[12] Billovits GF, Durning CJ. Polymer 1988;29:1468.
[13] Blackadder DA, Vincent PI. Polymer 1974;15:2.
[14] Miranda NR, Willits JT, Freeman BD, Hopfenberg HB. J Membrane Sci 1994;94:67.
[15] Park JY, Paul DR, Haider I, Jaffe M. J Poly Sci: Poly Phys Ed 1996;34:1741.
[16] Cohen MH, Turnbull D. J Chem Phys 1959;31:1164.
[17] Reid RC, Prausnitz JM, Polling BE. The properties of gases and liquids, 4th ed. New York: McGraw-Hill, 1987:741.
[18] Cantress GR, Freeman BD, Hopfenburg HB, Makhija S, Haider I, Jaffe M. In: Carfagna C, editor. Liquid crystalline polymers. Tarrytown, NY: Pergamon, 1994:233.
[19] Felder RM, Huvard GS. In Fava R, editor. Methods of experimental physics, vol. 16C. New York: Academic Press, 1978:315.
[20] Lawton EL, Rigwald EL. In: Brandup J, Immergut EH, editors. Polymer handbook. New York: Wiley, 1989:V/101.
[21] Billmeyer FW. Textbook of polymer science, 3rd ed. New York: Wiley, 1984:578.
[22] Cheng SZD, Wunderlich B. Thermochimica Acta 1988;134:161.
[23] Murthy NS, Correale ST, Minor H. Macromolecules 1991;24:1185.
[24] Shen H-C. Master's Thesis. North Carolina State University, 1993.
[25] Hoffman DC, Caldwell JK. Proceeding of specialty polyesters 1995:223.
[26] VanAmerongen GJ. Rubber Chem Tech 1964;37:1065.
[27] Bondar VI, Freeman BD, Pinnau I. Proceedings of the American Chemical Society, Division of Polymeric Materials: Science and Engineering, Las Vegas, American Chemical Society, Division of Polymer Science: Materials and Engineering 1997;77:311.
[28] Singh A. Ph.D. Dissertation, North Carolina State University, 1997.
[29] Michaels AS, Vieth WR, Barrie JA. J Appl Phys 1963;34:1.
[30] Koros WJ, Paul DR. J Poly Sci Poly Phys Ed 1978;16:2171.
[31] Myers AW, Rogers CE, Stanett V, Swarc M. Modern Plastics 1957;34:157.
[32] Michaels AS, Bixler HJ. J Polym Sci 1961;50:393.
[33] Sanders ES. Ph.D. Dissertation, North Carolina State University, 1983.
[34] Crank J, Park GS. In: Crank J, Park GS, editors. Diffusion in polymers. New York: Academic Press Inc., 1968:1.
[35] Crank J. Mathematics of diffusion, 2nd ed., Oxford: Oxford Science Publications, 1975:414.
[36] Berens AR, Hopfenberg HB. Polymer 1978;19:489.
[37] Kishimoto A, Fujita H, Odani H, Kurata M, Tamura M. J Phys Chem 1960;64:594.
[38] Billovits GF, Durning CJ. Polymer Commun 1990;31:358.
[39] Berens AR, Hopfenberg HB. Polymer, 1978;19:481.
[40] Bevington P. Data reduction and error analysis for the physical sciences. New York: McGraw-Hill, 1969:150.
[41] Fleming GK, Koros WJ. Macromolecules, 1986;19:2285.
[42] Miranda N. Ph.D. Dissertation, North Carolina State University, 1992.
[43] Kujita H. In: Crank J, Park GS, editors. Diffusion in polymers. New York: Academic Press, 1968:75.
[44] Ghosal K, Freeman BD. Poly Adv Tech 1994;5:673.
[45] Paul DR, Koros WJ. Poly Sci: Poly Phys Ed 1976;14:675.
[46] Stern SA, Saxena V. J Membrane Sci 1980;7:47.
[47] Vrentas JS, Duda JL. J Polym Sci: Polym Phys Eds 1977;15:403.